ACS OMEGA

http://pubs.acs.org/journal/acsodf

Article

Inhibition Of Tau Protein Aggregation By a Chaperone-like β-Boswellic Acid Conjugated To Gold Nanoparticles

Masoumeh Gharb, Amideddin Nouralishahi, Ali Riazi, and Gholamhossein Riazi*

Cite This: *ACS Omega* 2022, 7, 30347−30358

Read Online

ACCESS | Metrics & More | Article Recommendations | Supporting Information

ABSTRACT: A potential therapeutic strategy to inhibit tau protein aggregation in neurons has substantial effects on preventing or controlling Alzheimer's disease (AD). In this work, we designed a covalent and noncovalent conjugation of β-boswellic acid (BA) to gold nanoparticles (GNPs). We provided the opportunity to investigate the effect of the surface composition of BA-GNPs on the aggregation of the tau protein 1N/4R isoform in vitro. HR-TEM and FESEM micrographs revealed that GNPs were spherical and uniform, smaller than 25 nm. According to UV−visible and FTIR data, BA was successfully conjugated to GNPs. The finding illustrates the effect of the surface charge, size, and hydrophobicity of BA-GNPs on the kinetics of tau protein aggregation. The size and surface area of U-G-BA demonstrated that inhibited tau aggregation more effectively than covalently linked BA. The proposed method for preventing tau aggregation was monomer reduction. At the same time, a chaperone-like feature of GNP-BA while sustaining a tau native structure prevented the additional formation of fibrils. Overall, this study provides insight into the interaction of GNP-BAs with a monomer of tau protein and may suggest novel future therapies for AD.

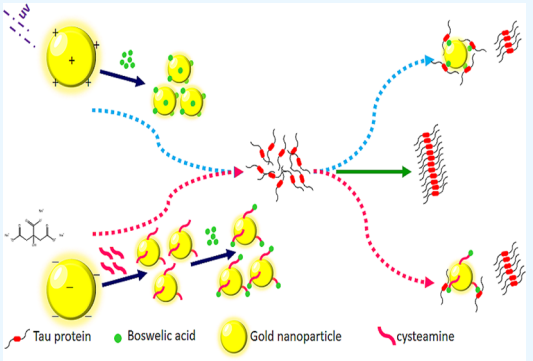

INTRODUCTION

Alzheimer's disease (AD) is the most common form of dementia in the elderly worldwide, and its prevalence is increasing in tandem with life expectancy.[1] The formation of amyloid-beta (Aβ) plaques and tau neurofibrillary tangles are two main hallmarks of AD pathology associated with other disease processes including neuroinflammation, mitochondrial dysfunction, and neurotransmitter shortfalls.[2,3] The tau protein is a member of the microtubule-associated protein (MAP) family. The accumulation of tau protein's paired helical filaments (PHFs) causes dynamic instability in microtubule protein (MT). Destabilization of MT disturbs axonal transport, leading to a memory and learning deficit.[4−9] Tau protein has a natively unfolded structure with two domains with different charge distributions. The charge distribution in the N-terminal domain is negative, whereas the charge distribution in the C-terminal domain is positive. The C-terminal segment of the tau protein plays a major role in the tau protein aggregation to paired helical filaments (PHFs). According to earlier studies, particular charge−charge and hydrophobic interactions of the amyloid−polypeptide structure are crucial for the development of oligomeric states. Therefore, tauopathy may have powerful importance in AD progression and a method focused on tau pathology may be effective for AD therapeutics.[10,11]

Experimental and clinical studies have suggested the beneficial effects of herbal medicine in neurodegenerative conditions.[12−14] Previous studies have indicated that plant-derived terpenoids positively affect neurodegeneration.[15] BAs are triterpenoid and hydrophobic compounds extracted from the resin of Boswellia plant species and they possess anti-inflammatory, antioxidant, and antiedema properties.[16−19] It has been shown that BA can ameliorate memory deficit in animal AD models.[20] However, their mechanism of action is not clearly understood.[14,16] Previous studies showed BA possesses therapeutic potential in the tau protein and in microtubule stability, including in Alzheimer's disease.[21,22] The therapeutic application of BA has been limited because of its low aqueous solubility and bioavailability. BA is linked to nanoparticles (NPs) to overcome these limitations.[23]

Nanotechnology-based methods and materials for diagnosing and treating neurodegenerative diseases have been developed. The combined nanoscience and pharmaceutical science application is very promising and has multiplied recently. Therefore, there has been a huge demand for the use of NPs in the last few decades.[24−26] Metal-based NPs, such as gold NPs (GNPs), are readily synthesized in various sizes and shapes, easily functionalized, and considered inert and highly stable against oxidation in biological environments and

Received: June 9, 2022
Accepted: July 28, 2022
Published: August 18, 2022

Scheme 1. (a) Schematic of the Cross-Linking GNP Reactions with BA Functionalized by EDC/NHS in Covalent Conjugation; (b) Schematic of the Noncovalent Conjugation of GNPs with BA

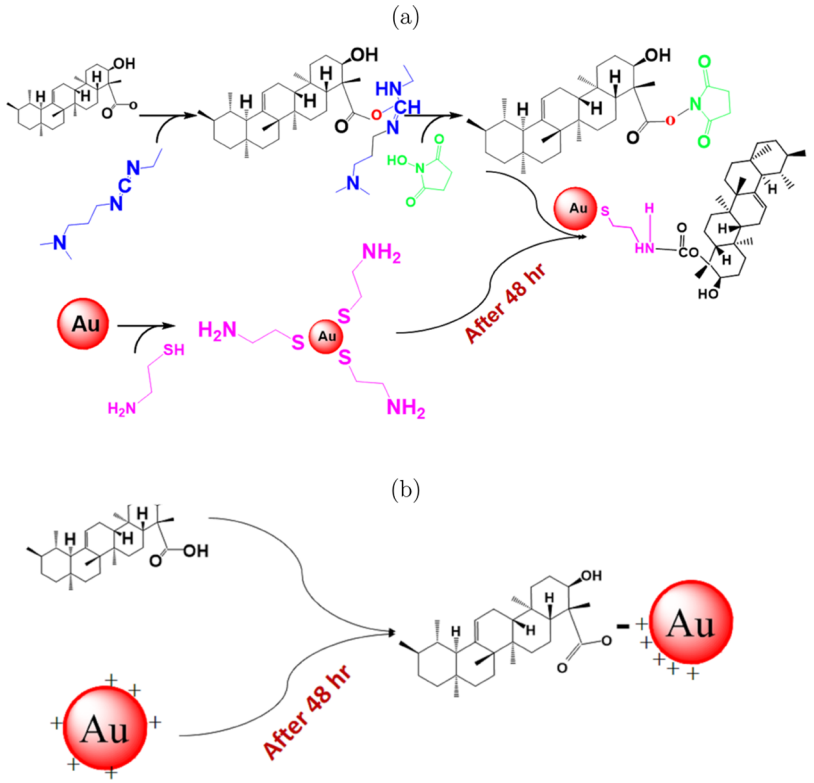

crossing the blood−brain barrier.[27,28] GNPs are generally considered to be nontoxic[29] and biocompatible with a high surface-area-to-volume ratio[30] and can be functionalized with a high density of ligands for drug delivery.[31−34]

The NP shape, size, hydrophobicity−hydrophilicity, surface charge, surface area, and surface chemical groups play a crucial role in determining the effect of NPs on protein aggregation. A wide range of possibilities may arise on both sides. The first element of biological systems is proteins, which encounter NPs upon arrival, where they are most welcomed by the protein-provided corona. As a result, in an NP−protein complex, protein binding to the surface of the NPs is not shocking.[35,36] The bonding may result in conformational changes in the adsorbed proteins, regardless of the state of the protein (from a folded or unfolded monomer to larger assemblies like fibrils). In this instance, the protein aggregation kinetics will be accelerated or inhibited.[37]

Inhibition of tau protein aggregation by employing metal NPs has been examined, suggesting that GNPs may also exert disaggregation activity.[35] Therefore, in the following investigation, the effects of hydrophobicity, size, and charged surface GNP-BA on the monomer of tau protein aggregation were examined. Subsequent inhibition of tau protein aggregation by GNP-BA highlighted the impact of hydrophobic surfaces in a chaperone-like mechanism.

RESULTS AND DISCUSSION

Preparation and Characterization of GNP-BA Nanoparticles. The Turkevich method and photochemical protocol have been broadly utilized as standard methods for GNP synthesis to develop biotechnological purposes.[38,39] The chemical synthesis procedure involving bioconjugating the GNPs (C-G) to BA (C-G-BA) through carbodiimide chemistry is illustrated in Scheme 1A.[40] BA was conjugated on the surface of cysteamine-GNPs via amide bonding between the amino groups on the surface of cysteamine-GNPs and the carboxylic groups of BA that were activated by EDC/NHS. BA conjugation on the surface of GNPs also enhances their bioavailability, and various physicochemical criteria needed for biological applications are offered. Contrarily, the more stable method in this faction is covalent conjugation. However, the majority of research that used in situ, noncovalent bonding-based methods appeared successful,[41] whereas noncovalently electrostatic interaction coated the physically prepared GNPs (U-G) with BA (Scheme 1b). It is important to note that these appealing surfaces have the potential to influence fibril formation.

We characterized the proper formation and conjugation of GNPs with BA using UV−vis spectra (Figure 1a). A surface plasmon band at 522 nm was detected that indicated stable C-G formation. After treatment with BA, it redshifted to 525 nm. Similarly, a surface plasmon band at 530 nm for physically prepared U-G redshifted to 536 nm after loading of BA onto U-G nanoparticles (U-G-BA). UV absorption studies of GNP-BAs exhibiting a redshift show it is related to a change in the dielectric environment of the NPs, thus indicating successful conjugation of BA-GNP. Furthermore, the difference in the surface plasmon bands and redshift, respectively, were related to the larger diameter of U-G and utilized conjugation methods.[40,42]

DLS (Figure 1b) and ζ potential results of C-G were ∼23.4 nm and −25.59 ± 2.02 mV. For C-G-BA, the hydrodynamic diameter was increased to ∼27.4 nm, and ζ potential was reduced to −15.74 ± 0.76 mV. Following the covalent conjugation, the increased ζ potential was due to cysteamine

https://doi.org/10.1021/acsomega.2c03616
ACS Omega 2022, 7, 30347−30358

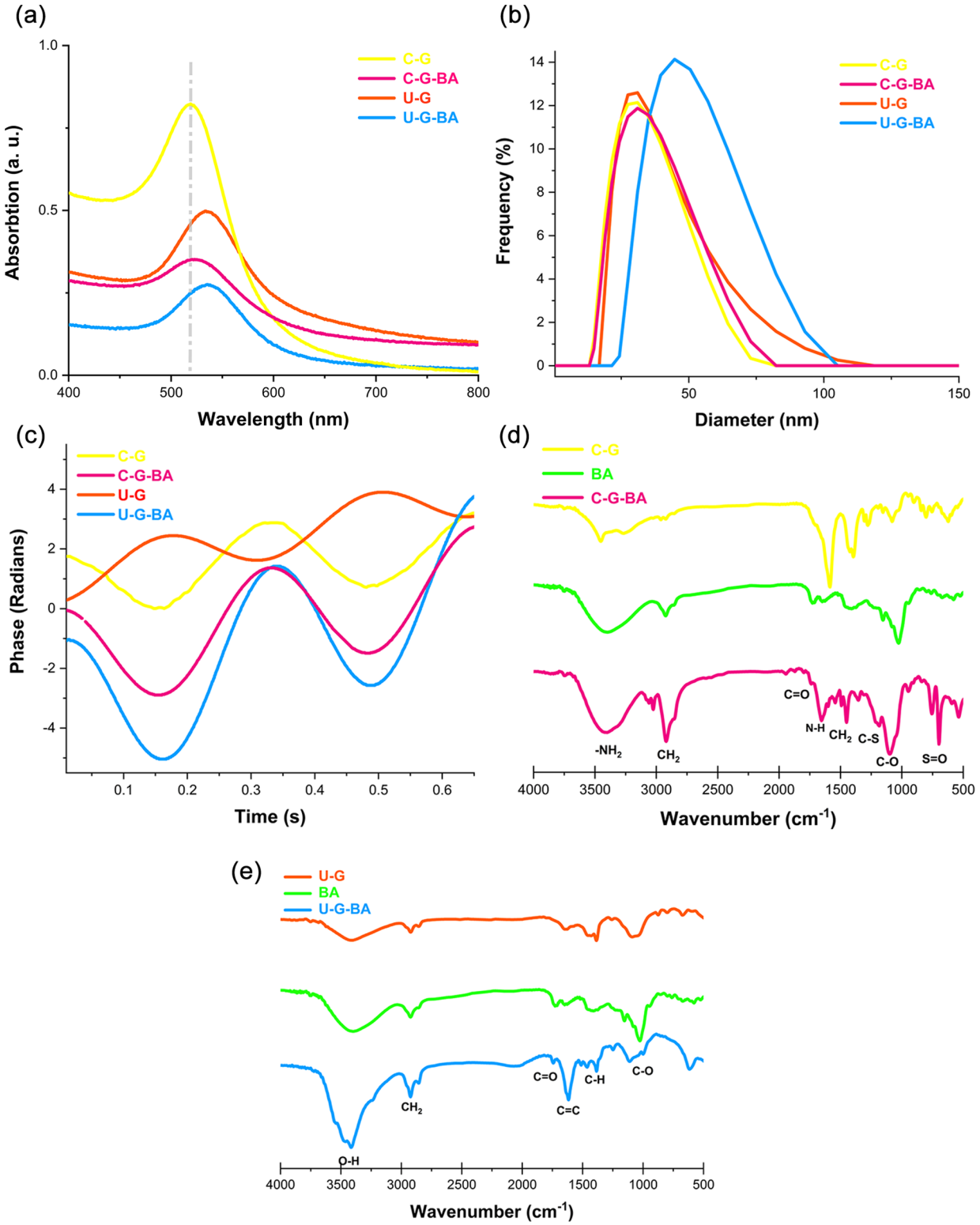

Figure 1. (a) UV−vis absorption spectra, (b) histograms of size distribution, (c) zeta potential of the phase diagram of GNP and GNP-BA. FT-IR spectra of (d) C-G, BA, and C-G-BA and (e) U-G, BA, and U-G-BA.

(cationic), cross-linking agent EDC (cationic carrier)/NHS, and BA (ionic) addition to C-G. The BA addition presented a less negative charge than expected. It might be due to the impurities and less BA binding to C-G. Following binding to negatively charged carboxyl groups of BA by electrostatic interactions, a reduction in the ζ potential charge was observed. The DLS and ζ potential results of U-G were ∼48.2 nm and +8.16 ± 0.86 mV. For U-G-BA, the hydrodynamic diameter was increased to ∼55.5 nm, and ζ potential was reduced to −22.56 ± 1.51 mV. U-G had a larger diameter than C-G, so the number of BA equivalents might be higher consequently. Our DLS study indicated a uniform size that was increased in diameter when it conjugates with BA. The stability of the synthesized GNPs and conjugated to BA

https://doi.org/10.1021/acsomega.2c03616
ACS Omega 2022, 7, 30347−30358

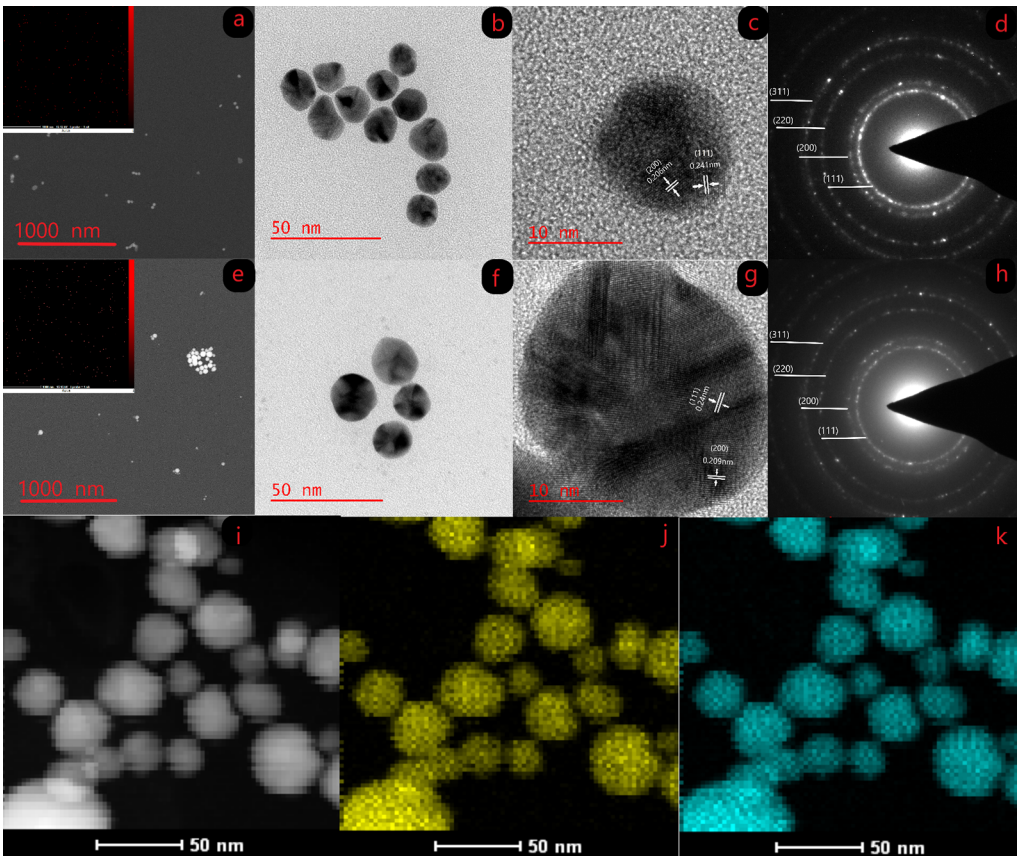

Figure 2. (a) FESEM image of the distribution of spherical C-G with the EDS map analysis in the inset. (b) TEM image for C-G and its size distribution. (c) HR-TEM image of C-G. (d) Selected area electron diffraction (SAED) pattern. (e) FESEM image of the distribution of spherical U-G and the EDS map analysis in the inset. (f) TEM image of U-G and size distribution. (g) HR-TEM image of U-G. (h) Selected area electron diffraction (SAED) pattern. (i–k) TEM-EDX of GNPs.

was measured by the phase plot of the ELS ζ potential analyzer, which illustrates good stability. The phase sign of U-G synthesized NPs, as shown in Figure 1c, was inverted because of the electrostatic bond of BA onto the surfaces of the photochemically synthesized NPs.

To further study the functional groups on the surface of GNPs, we measured the FT-IR spectra of C-G, BA, and C-G-BA (Figure 1d). Conjugation of BA onto the surface of C-G leads to the representation of additional peaks at 1658, 1600, and 3402 cm^{-1} that are attributed to the C═N amine, the amide II band, and the primary amine band corresponds to the formation of amide bonds between C-G and BA. The FT-IR spectra of U-G, BA, and U-G-BA are shown in Figure 1e. U-G was observed to be similar to C-G. Bands of U-G-BA are shown at 1026 cm^{-1}, which is associated with C−O stretching removed, and 1637 and 1724 cm^{-1}, which are ascribed to C═C stretching in the aromatic ring and increased C═O stretching, respectively.[43,44]

We further performed electron microscopy to illustrate the surface morphology of the GNP synthesized C-G (Figure 2a) and U-G (Figure 2e) and showed that C-G and U-G were rather homogeneous in size and shape. The size of the NPs was characterized by means of TEM around ∼13 nm for C-G (Figure 2b) and 24 nm for the U-G (Figure 2f). The selected area electron diffraction (SAED) pattern of C-G (Figure 2c) and U-G (Figure 2g) indicated that the NPs were pure crystalline in nature. Diffraction patterns were obtained from HR-TEM with pure GNP (JCPDS Card No. 0784−04) and Bragg's law was used to evaluate the D spacing. Finally, the corresponding data planes (hkl) were shown (Table S1). In conclusion, these findings support a crystalline phase of the synthesized GNP being composed of an inverted spinal structure.[45,46] FESEM, HR-TEM, and the EDX map confirmed the purity of elemental gold NPs (Figure 2a, e, i–k).[47]

Characterization of Drug Loading Efficiency. The drug loading content (DL) of C-G-BA and U-G-BA were calculated using the following equation:[48]

$$\mathrm{DL\ (mg/mg)} = \frac{\text{Weight of the drug in nanoparticles}}{\text{Weight of the nanoparticles}} \quad (1)$$

DL was calculated as 0.020 and 0.026 for the C-G-BA and U-G-BA, respectively. The number of BA loaded on the U-G-BA was higher than that on the C-G-BA.

Tau Protein Aggregation and Fibrillation. The tendency of tau protein to aggregation in the presence of heparin has been well reviewed. Therefore, the ThT assay was used to track the kinetics of tau protein fibrillation. Kinetic parameters have been estimated by fitting a sigmoid curve (equation), which is commonly used to explain the kinetics of amyloid aggregation regardless of protein type.[49]

$$F = \frac{F_{\mathrm{final}} - F_0}{1 + \exp(-k_{\mathrm{app}}(t - t_{1/2}))} \quad (2)$$

Where F is the fluorescence intensity at time t and F_0 and F_{final} indicate the initial and final fluorescence intensity in order.

https://doi.org/10.1021/acsomega.2c03616
ACS Omega 2022, 7, 30347−30358

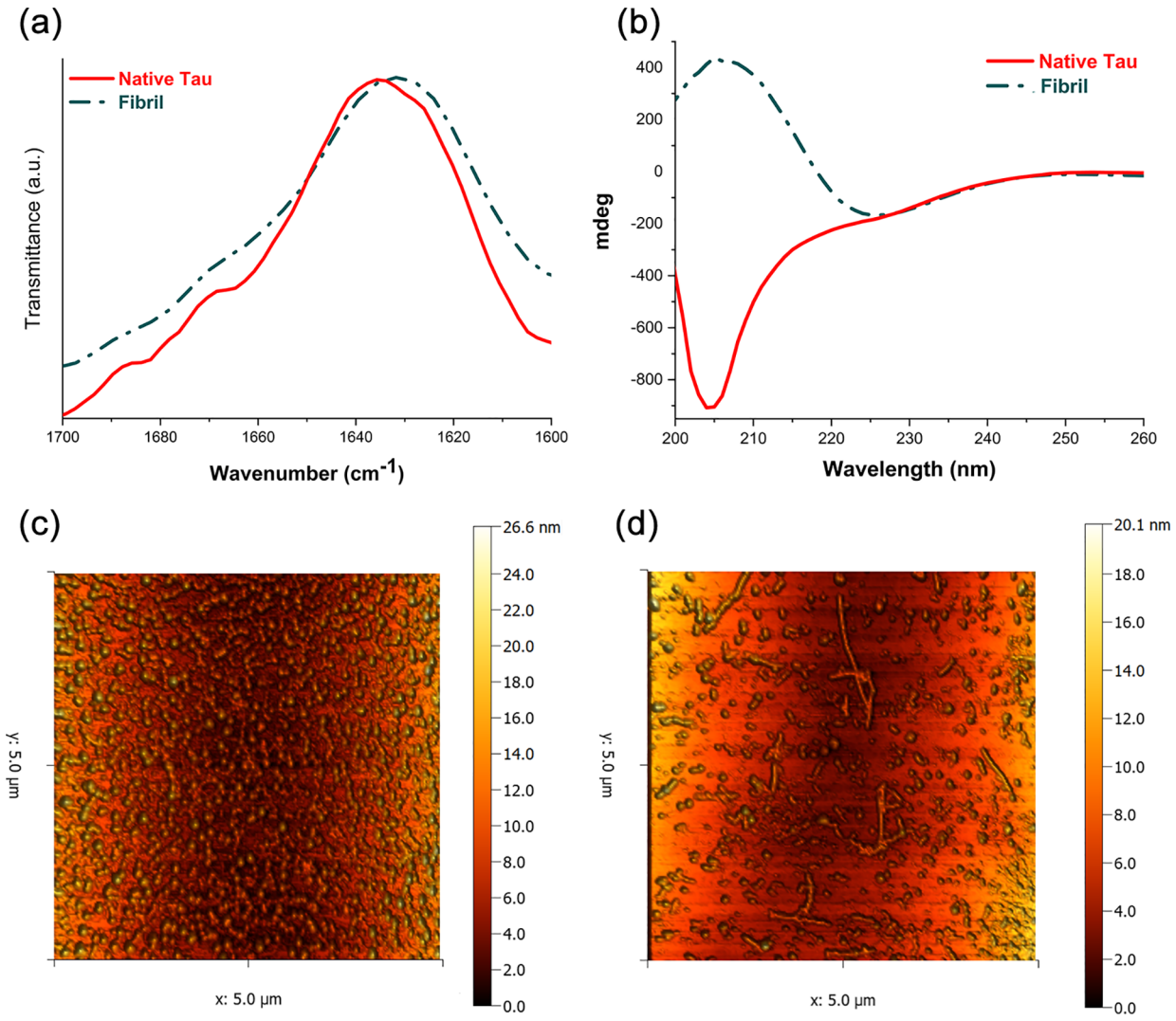

Figure 3. Tau protein structural analyses in native and fibril states: (a) ATR−FTIR and (b) far-UV CD. AFM image of (c) native tau and (b) tau fibril.

Furthermore, $t_{1/2}$ is the needed time for the formation of half of the protein aggregation amounts, and k_{app} is the evident aggregation constant so that the lag time can be calculated. Predicting the fibrillation lag time in the presence of dynamic inhibitors would be useful. Fragmentation and other molecular processes including inhibition and off-pathway aggregation are thought to have a substantial influence in the fibril formation's lag phase.[50]

To quantify the lag phase for our system of nucleated self-assembly, we used the formal explanation in which we recognize the time at which the growth rate is the highest, indicate the tangent at that point, and finally take its time intercept as the lag time.[51] Tau protein fibrillation kinetics are shown, and the apparent protein aggregation constants are mentioned (Table S2). Tau protein fibrillation kinetics started with a short apparent lag phase that could be fitted by a polynomial function, followed by a plateau phase. The findings revealed that the conformational changes required for tau protein fibrillation differed from those required for aggregation in vitro.[52] The secondary structure of the tau protein as shown by far-UV CD was consistent with previous research.[52,53] The CD spectra of tau protein monomers (random coil structure) (Figure 3a) had a characteristic, strong minimum at 200 nm and a maximum at 220 nm, which is consistent with a random coil conformation. The ThT fluorescence data at the end of fibrillation process indicate that tau protein monomers are converted to fibrils, and the CD spectrum showed changes in the wavelength and intensity of the maximum and minimum due to changes in the tau protein secondary structure.[54]

This demonstrated the formation of a β-sheet structure. Thus, ATR−FTIR was provided as further evidence (Figure 3b). FTIR has a strong ability to detect changes in protein secondary structures for amide I. Amide I arises from stretching vibrations of carbonyl amide groups. ATR-FTIR spectra recorded for the native and fibrillar forms of the tau protein are presented. In the native tau protein, a maximum of about 1631 cm^{-1} random coil predominances identified by previous studies were elucidated. Even stronger conformational changes occurred during fibrillation, such that the random coil of the native tau protein has a narrow amide I maximum at about 1645 cm^{-1} PHFs.[55]

AFM images show different stages of native tau protein (Figure 3c) and tau protein fibrillation (Figure 3d): primarily, the tau proteins are generated in oligomers as building blocks that line up side by side to organize higher-order intermediates. Spherical entities, which are a characteristic of oligomers, were

https://doi.org/10.1021/acsomega.2c03616
ACS Omega 2022, 7, 30347−30358

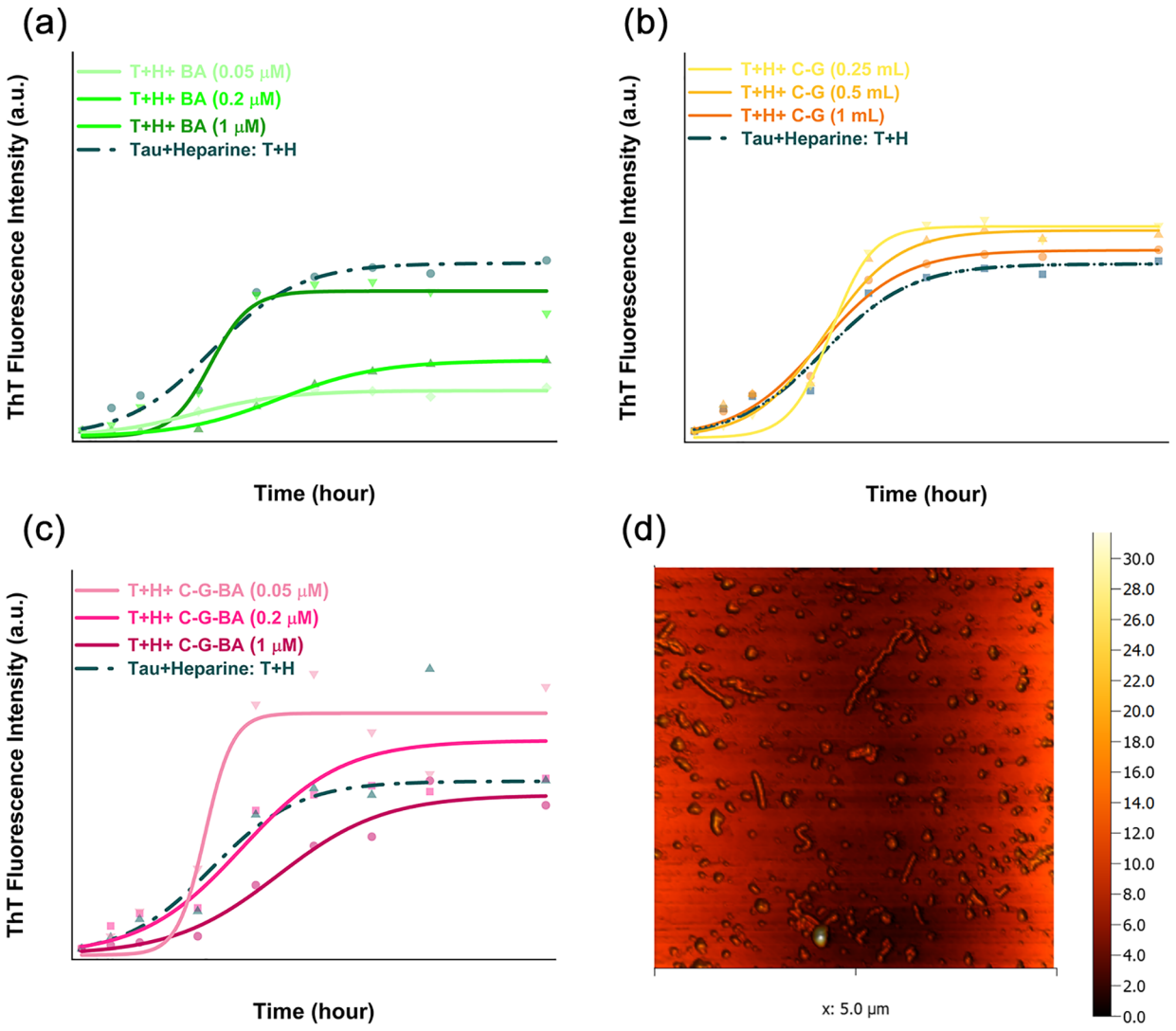

Figure 4. Aggregation rate of tau protein in the presence of chemically prepared GNPs, measured by ThT assay. Effect of the (a) BA concentration (0.05−1 μM), (b) C-G concentration (0.25−1 mL), and (c) C-G-BA concentration (0.05−1 μM). (d) AFM image tau treatment with C-G-BA.

detectable right from the start of the fibrillation process. The above oligomers have been identified as polymorphic structures that initiate protofibril formation. Ultimately, the maturation of protofibrils led to the formation of well-organized fibrillation.[56,57]

Effect of GNP-BAs on Tau Protein Aggregation and Mechanism of Inhibition. The complex tau protein−tau protein, GNP−tau protein, and GNP−GNP interactions determine the final outcome of the NP−protein system. It was inferred by the GNP−BA impacting tau protein aggregation/fibrillation dynamics that there was a helpful NP−protein interaction; however, the exact mechanism is unknown.[58] Consequently, when examining the inhibitory mechanism of GNP−BA on tau protein aggregation, the two most likely theories were chosen to concentrate on: (1) protein binding to the surface of GNP−BA causes protein monomer reduction and (2) chaperone-like activity of GNP−BA minimizes the conformational changes necessary for stimulating the process. ThT fluorescence was used to monitor the kinetics of tau protein aggregation in the presence of BA, GNP, and GNP-BA during incubation. Use a suitable single exponential function, the ThT fluorescence values were plotted versus time (lag time is required to activate the time to nucleation, which is required to form an ordered, stable nucleus). Then, fibril elongation occurs rapidly as a result of the association of monomers or oligomers by a combination of various interactions. Furthermore, controlled by several types of noncovalent forces/interactions.[59,60] The apparent lag time, rate constants, and final fibril extent of tau protein aggregation were determined and listed from related exponential plots (Table S2). ThT emission sigmoidal curves were seen during tau protein incubation with all different BA doses (0.05−4 μM) (Figures 4a and 5a).

BA clearly showed a pattern of dose-dependent accelerated fibrillation. Lower concentrations of BA (0.05−4 μM) reduced fibrillation by decreasing the nucleation lag time. Conversely, unlike with the aggregation experiments, elongation was affected by the addition of BA in the presence of more than 20 μM BA. ThT fluorescence analysis showed the optimum concentration of BA (0.05 μM) to inhibit tau protein aggregation. The results of different concentrations of U-G (0.25−1 mL) are shown in Figure 4b. U-G resulted in the induction of aggregation in a dose-dependent manner. This indicates that there is a relationship between the tau protein

https://doi.org/10.1021/acsomega.2c03616
ACS Omega 2022, 7, 30347−30358

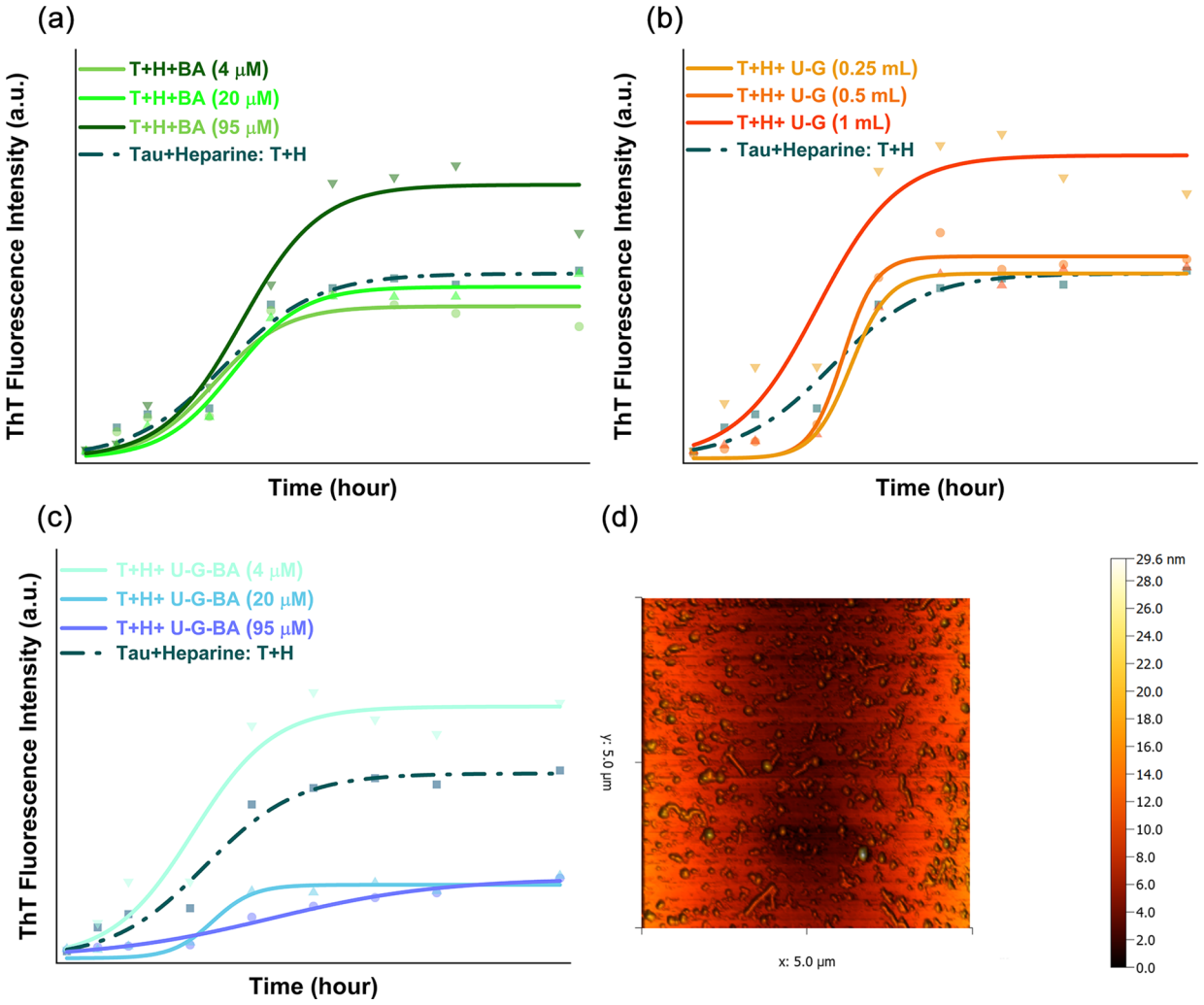

Figure 5. Aggregation rate of the tau protein in the presence of physically prepared GNPs, measured by ThT assay. Effect of the (a) BA concentration (4−95 μM), (b) t U-G concentration (0.25−1 mL), and (c) U-G-BA concentration (4−95 μM). (d) AFM image of tau treatment with U-G-BA.

binding to the surface of U-G, which can lengthen the lag time (by lowering the solution concentration such that the essential nuclei cannot form), and the impact of the positive charge on the conformation of the adsorbed tau protein. A possible explanation for this result could be the physical interaction between a positively charged U-G and a negatively charged tau segment (C-terminal).[61] This interaction increases the local concentration of tau protein, which facilitates filament nucleation on its surface and efficiently accelerates the formation of tau protein. The effect of different concentrations of C-G (0.25−1 mL) are shown in Figure 5b, C-G-BA (0.05−1 μM) in Figure 4c, and U-G-BA (4−95 μM) in Figure 5c.[62] These NPs were illustrated to have a dose-dependent efficacy on tau protein fibrillation. Opposite of the positive U-G, the negative C-G, C-G-BA, and U-G-BA are demonstrated to delay or inhibit the fibrillation process in a dose-dependent manner. The fibrillation process was effectively inhibited with GNP-BA. Therefore, it has been shown that the inhibitory effect of GNP-BA is greatly dependent on the surface composition of the GNP. At high concentrations of GNP-BA, the lag phase was increased, which shows a delay time at which the primary nuclei could emerge. Because apolar residues typically compose about 30−50% of total proteins, remarkable amounts of protein self-recognition and assembly must be derived from hydrophobic interactions.[63] The significant deceleration is presumably caused by the interaction between the hydrophobic segment of tau and the negatively charged GNP-BA surface.[64] Moreover, GNP-BA could be caused by interactions between the hydroxyl group of BA and the hydrophobic residues of the tau protein monomers or oligomers, leading to an uneven situation for fibril formation. More specifically, we proposed that negatively charged GNP-BA can interact with the amide backbone of the tau protein core (N-terminal).[65] The inhibition of tau protein aggregation involves the absorption of monomeric tau protein by the surface of the GNP-BA so that the free monomer tau protein decreases within the solution, shifting the equilibrium away from fibrillation because a critical monomer concentration is needed to initiate aggregation, causing an increase in the time required for nucleation to happen. Moreover, in the phases of polymerization, the elongation phase increased and there was a reduction in tau protein aggregation. The kinetic parameters F_{final} (aggregation extent) and K_{app} (elongation phase) decrease with an increase in the concentration GNP-BA, whereas $t_{1/2}$ (lag time) increases.[56,66−70] Overall, it can be deduced that NP displays a dual manner that interferes with the protein amyloid

https://doi.org/10.1021/acsomega.2c03616
ACS Omega 2022, 7, 30347−30358

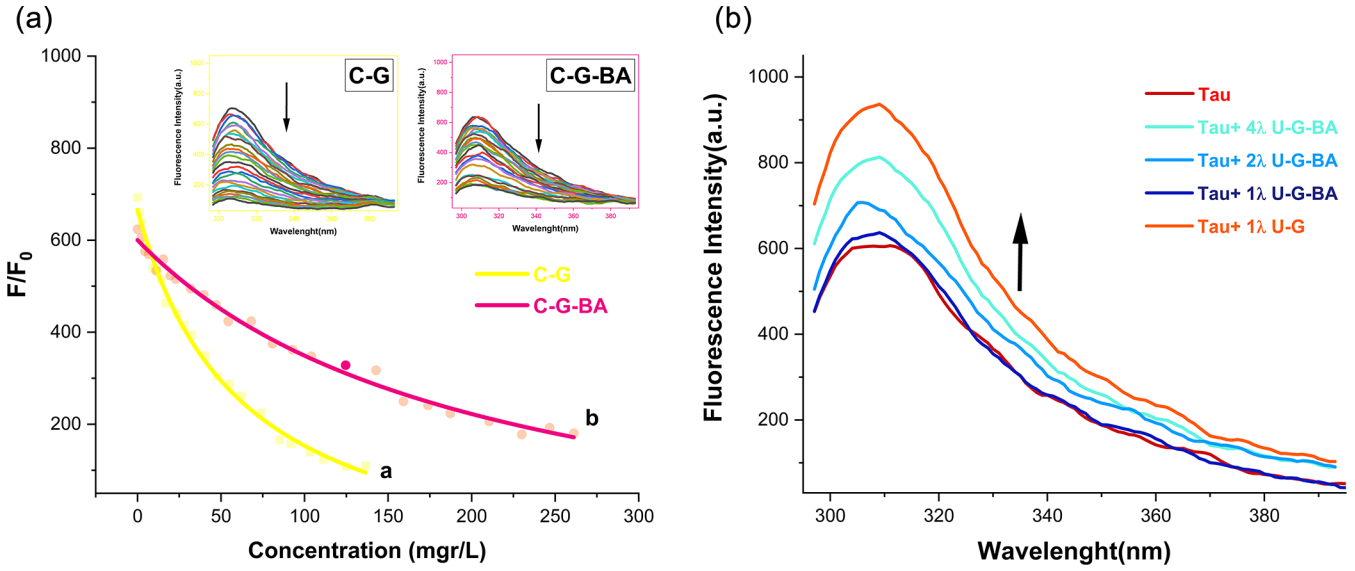

Figure 6. Intrinsic fluorescence quenching of tau in the presence of (a) C-G and C-G-BA and (b) U-G and U-G-BA at room temperature.

formation. In our study, the highest efficacy of U-G-BA in the inhibition of tau protein aggregation might be due to the larger diameter of U-G, and possibly higher amounts of the BA carried on U-G compared to C-G.[71] The CD spectra data of tau fibrillation in the presence of BA, GNP, and GNP-BA confirmed the ThT fluorescence results (Figure S1).[54] These results are further supported by our AFM studies on C-G-BA (Figure 4d) and U-G-BA (Figure 5d). Treatment of tau proteins with GNP-BA resulted in a few dispersed higher-order oligomers (remarkably smaller and less than what the tau fibrillation assessed), which were the most observed assembled entities. Further, we observed the presence of spherical shapes, possibly due to the interaction of tau protein with GNP-BA that formed these spherical shapes.[56,57]

GNP-BA inhibited the formation of the fibrillar PHFs. To further understand the interaction of BA loaded with NPs with tau protein, we performed a binding assay. K_D values were measured and determined to be 203.55 for C-G-BA and 66.48 for C-G, indicating a higher binding affinity of C-G-BA to tau protein (Figure 6a and Table S3). we could not measure K_D because of the increasing intensity of U-G and U-G-BA (Figure 6b).

The tryptophan signal in the tau samples from adding U-G and U-G-BA had an increasing trend up, showing that more hydrophobic complexes were formed.[52] These SDS-PAGE results affirm that GNPs-BA can effectively bind to tau.

On the basis of the results, this manner of GNP-BA could be categorized as having a chaperone characteristic. According to this, it has been found that clusterin, an extracellular chaperone, prevents the formation of tau fibrils by stabilizing tau monomers and interacting with their high-molecular-weight oligomers. This chaperone function of GNP-BA thereby increases the hydrophobicity of their surface.[72]

Conclusion. This study constructed a BA conjugated to GNPs that can prohibit tau protein aggregation, which can be administered to treat AD. Both methods of GNP synthesis used resulted in a spherical and hemogenic size. FTIR illustrated the BA load on GNP through covalent and noncovalent conjugation. GNPs conjugated to BA interact with tau protein through a rhythmic binding process. This interaction prevented tau protein dimerization by reducing tau−tau protein interaction, leading to tau−nuclei oligomerization and delaying the polymerization of tau protein amyloid aggregates. U-G-BA demonstrates more efficiency in preventing aggregation compared to C-G-BA based on the higher loading of BA and the purity in the synthesis method and noncovalent conjugation. Research on the transmission across the blood−brain barrier (BBB) and in vivo studies in animal models to prove the inhibitory effect of U-G-BA on tau protein aggregation and the possibility of its future therapeutic application for Alzheimer's disease is ongoing.

MATERIALS AND METHODS

Materials. Gold(III) chloride trihydrate, 1-ethyl-3-(3dimethylaminopropyl) carbodiimide (EDC), N-hydroxy succinimide (NHS), 2-(N-111Morpholino) ethane sulfonic acid (MES), trisodium citrate, dimethyl sulfoxide (DMSO), thioflavin T (ThT), isopropyl-D-1-thiogalactopyranoside (IPTG), and the resin of SP sepharose gel were purchased from Sigma-Aldrich (Munich, Germany). Tween 20, 1,4-dithiothreitol (DTT), and Triton X-100 (TX-100) were purchased from Merck (Darmstadt, Germany). Boswellic acid was a gift from Kondor Pharma Inc. (Canada). Heparin (M.W. 15 000 Da), was purchased from Santa Cruz Biotechnology, USA. Deionized water was used for making all solutions.

Preparation of GNP-BAs Using the Chemical Method. GNPs were prepared using the Turkevich method.[38] Briefly, 1.5 mL of trisodium citrate (1%) was added to 25 mL of boiling chloroauric acid solution (0.8 mM) with vigorous stirring until its color changed from yellow to red. The reaction was completed within 15 min. The obtained colloidal suspension was slowly cooled to room temperature. EDC/NHS cross-linking chemistry was used to bind BA to GNPs covalently. Initially, 10 mL of GNPs were mixed with 22 μL of Tween 20 (20 μM) for 1 h. Then, 0.5 mL of the GNPs solution was mixed with cysteamine at 1 μM and dispersed in MES buffer (10 mM, pH 5.3). Next, the EDC (2 μM) was added to BA at 1 M concentration and was dispersed in MES buffer after 30 min under continuous shaking conditions. In the last step, (1 mL) of cysteamine-coated GNPs were added to the solution, NHS (4 μM) was added and shaken vigorously

https://doi.org/10.1021/acsomega.2c03616
ACS Omega 2022, 7, 30347−30358

for 48 h at room temperature. The solution was centrifuged at 10 000 × *g* for 30 min to remove excess EDC/NHS and unconjugated BA and stored at 4 °C.

Preparation of GNP-BAs Using the Physical Method. To prepare GNPs, we added 3 mL of HAuCl4 solution (3 mM) and TX-100 (5 mM) to a quartz cuvette 4 × 1 cm. The cuvette was placed directly under a UV light source (15 W) at a distance of 3 cm. After 10 min of irradiation, the solution turned red. To conjugate GNPs with BA, 0.5 mL of GNPs were mixed with BA (5 mM solution in DMSO) and incubated at room temperature on a rotator for 48 h. The solution was then centrifuged at 10 000 × *g* for 30 min to remove the excess and unconjugated BA and then stored at 4 °C.

Physicochemical Properties of GNP and GNP-BA. The spectra GNP and GNP-BA are measured by a UV−vis spectroscopy (Carry 100 Bio Varian) spectrophotometer. An FT-IR spectroscope (Irprestige-21, Shimadzu) was used for assessing the chemical interaction of different functional groups. The particle size, size distribution, and surface charge were analyzed by DLS and ζ potential (Brookhaven ZetaPlus ζ Potential Analyzer). The surface morphology, size distribution, and crystallinity of the GNP were examined using an HR-TEM microscope (FEI Tecnai G2 F20 SuperTwin) operating at a 200 kV accelerating voltage and an FE-SEM microscope (Zeiss Sigma VP). Images were analyzed using *ImageJ* software.

1N/4R-Tau Expression and Purification. The four-repeat isoform of the human tau protein (1*N*/4R-tau) was cloned and expressed in bacteria as previously described.[62] In brief, *E. coli* BL21 (DE3) carrying the recombinant pET-21a plasmid vector containing the His-tagged 4R-tau gene was cultured overnight at 37 °C with continuous shaking at 180 rpm in (10 mL) Luria broth (LB; 10 g/L yeast extract, 5 g/L NaCl, and 10 g/L bactotryptone, pH 7.4) and supplemented with 100 g/mL ampicillin. Bacterial culture was diluted 1:100 in LB media and grown until an optical density of 0.6 Expression of recombinant tau protein was induced by the addition of (1 mM) IPTG. Cells were harvested by centrifugation at 4000 × *g* for 20 min. The supernatant was discarded, resuspended in lysis buffer (20 mM Tris-HCl, 50 mM NaCl, 2 mM EDTA, 1 mM PMSF, pH 7.4), and sonicated at 4 °C. After centrifugation, it was boiled for 15 min, and then filtered supernatants were loaded onto the SP sepharose gel column. The SP sepharose gel column was washed with (20 mM Tris-HCl, 50 mM NaCl, pH 8.0). The tau protein was eluted using buffer (20 mM Tris-HCl, 1 M NaCl, pH 7.4). The protein concentration was determined using a Lowry assay, and its purity was evaluated by SDS-PAGE (98%).

Aggregation of Tau Protein. In brief, tau protein solution (45 μM) was treated with heparin (11.25 μM) in the presence of various concentrations of BA, GNP, and GNP-BA and incubated at 37 °C for 96 h. DTT (1 mM) was added daily to the samples.[73]

Thioflavin (ThT) Fluorescence Assay. A steady-state ThT kinetic assay with excitation at 440 nm and emission at 482 nm was recorded using a Cary Eclipse fluorescence spectrophotometer (Varian) to study the tau protein aggregation. Cuvette wells were filled with the final volume of the sample (200 μL) containing tau protein (45 μM) and ThT (20 μM).

Circular Dichroism (CD) Spectropolarimetry. The CD spectroscopy of the sample was recorded by a Jasco spectrometer (J−810) at room temperature between 200 and 260 nm, and then the obtained raw data representing the remaining molar ellipse were calculated. Secondary structure content was evaluated using *CDNN* software (version 2.1.0.233).

Attenuated Total Reflection−FTIR. ATR−FTIR measurements were performed using a Bruker Tensor 27 ATR with a resolution of 2 cm^{-1}. Native tau protein and aggregated samples were placed on the ATR crystal and the spectra were then recorded at room temperature; the obtained data were then baseline-corrected between 1700 and 1600 cm^{-1} for a more informative illustration.

Binding Assay. The ligand-binding affinity between GNP-BA was evaluated using fluorescence measurements at 25 °C.[74] Aliquots of the stock stock solution of GNP and GNP-BA were added to protein solutions to conduct a binding test. In each of the experiments, the concentration of tau protein was maintained at 45 μM, whereas the quencher concentrations varied.

The fluorescence spectra of tau protein were measured between 286−400 nm upon excitation at 276 nm. The excitation and emission slit width were adjusted to 5 and 10 nm, respectively. Data were fitted to obtained the dissociation constant of the ligand-binding site (K_D).

Sodium Dodecyl Sulfate-Polyacrylamide Gel Electrophoresis (SDS-PAGE). The inhibition of PHF assembly by GNP-BA was confirmed by loading the samples at end of time incubation intervals on 10% SDS-PAGE.

Atomic Force Microscopy (AFM). Native tau protein and end-incubation samples were diluted with distilled water (1:32 V/V), and 10 μL of each sample was located onto freshly cleaved mica and dried at room temperature. A Veeco Auto Probe CP Research was used at a frequency of 50 kHz and 15 N/m with a rounding tip radius of 10 nm.

■ ASSOCIATED CONTENT

Supporting Information

The Supporting Information is available free of charge at https://pubs.acs.org/doi/10.1021/acsomega.2c03616.

FTIR spectra results ; Table S1, data from HR-TEM; Table S2, kinetic parameters of GNPs; Table S3, binding parameters; Figure S1, changes in the tau protein structure during aggregation by CD spectroscopy; Figure S2, SDS-PAGE analysis (PDF)

■ AUTHOR INFORMATION

Corresponding Author

Gholamhossein Riazi − *Institute of Biochemistry and Biophysics, University of Tehran, Tehran 14176-14335, Iran;* orcid.org/0000-0001-5434-4042; Phone: +98 (0) 21 66956981; Email: ghriazi@ut.ac.ir

Authors

Masoumeh Gharb − *Institute of Biochemistry and Biophysics, University of Tehran, Tehran 14176-14335, Iran; Caspian Factually of Engineering, University of Tehran, Rezvanshahr 4386191836 Gilan, Iran*

Amideddin Nouralishahi − *Caspian Factually of Engineering, University of Tehran, Rezvanshahr 4386191836 Gilan, Iran*

Ali Riazi − *Kondor Pharma Inc., Mississauga, Ontario L4V 1T4, Canada*

Complete contact information is available at: https://pubs.acs.org/10.1021/acsomega.2c03616

https://doi.org/10.1021/acsomega.2c03616
ACS Omega 2022, 7, 30347−30358

Notes

The authors declare no competing financial interest.

■ ACKNOWLEDGMENTS

We thank Mohammad Reza Ashrafi-Kooshk, who provided insight and expertise that greatly assisted and guided the research, and Dr. Sogol Meknatkhah for comments that significantly improved the manuscript.

■ REFERENCES

(1) Delgado, A.; Cholevas, C.; Theoharides, T. C. Neuroinflammation in Alzheimer's disease and beneficial action of luteolin. *BioFactors* **2021**, *47*, 207−217.
(2) Alvariño, R.; Alonso, E.; Lacret, R.; Oves-Costales, D.; Genilloud, O.; Reyes, F.; Alfonso, A.; Botana, L. M. Caniferolide A, a macrolide from Streptomyces caniferus, attenuates neuroinflammation, oxidative stress, amyloid-beta, and tau pathology in vitro. *Mol. Pharmaceutics* **2019**, *16*, 1456−1466.
(3) Muralidar, S.; Ambi, S. V.; Sekaran, S.; Thirumalai, D.; Palaniappan, B. Role of tau protein in Alzheimer's disease: The prime pathological player. *Int. J. Biol. Macromol.* **2020**, *163*, 1599−1617.
(4) Dhanavade, M. J.; Sonawane, K. D. Amyloid beta peptide-degrading microbial enzymes and its implication in drug design. *3 Biotech* **2020**, *10*, 247.
(5) Sen, T.; Saha, P.; Jiang, T.; Sen, N. Sulfhydration of AKT triggers Tau-phosphorylation by activating glycogen synthase kinase 3β in Alzheimer's disease. *Proc. Natl. Acad. Sci. U. S. A* **2020**, *117*, 4418−4427.
(6) Guo, W.; Stoklund Dittlau, K.; Van Den Bosch, L. Axonal transport defects and neurodegeneration: Molecular mechanisms and therapeutic implications. *Semin. Cell Dev. Biol.* **2020**, *99*, 133−150.
(7) Vitet, H.; Brandt, V.; Saudou, F. Traffic signaling: new functions of huntingtin and axonal transport in neurological disease. *Curr. Opin. Neurobiol.* **2020**, *63*, 122−130.
(8) Barbier, P.; Zejneli, O.; Martinho, M.; Lasorsa, A.; Belle, V.; Smet-Nocca, C.; Tsvetkov, P. O.; Devred, F.; Landrieu, I. Role of Tau as a Microtubule-Associated Protein: Structural and Functional Aspects. *Front. Aging Neurosci.* **2019**, *11*, DOI: 10.3389/fnagi.2019.00204
(9) Mohammadi, F.; Takalloo, Z.; Rahmani, H.; Nasiri Khalili, M. A.; Khajeh, K.; Riazi, G.; H. Sajedi, R. Interplay of isoform 1N4R tau protein and amyloid-β peptide fragment 25−35 in reducing and non-reducing conditions. *J. Biochem.* **2021**, *169*, 119−134.
(10) Dafsari, F. S.; Jessen, F. Depressionan underrecognized target for prevention of dementia in Alzheimer's disease. *Transl. Psychiatry* **2020**, *10*, 160.
(11) Gao, J.; Chen, X.; Ma, T.; He, B.; Li, P.; Zhao, Y.; Ma, Y.; Zhuang, J.; Yin, Y. PEG-Ceramide Nanomicelles Induce Autophagy and Degrade Tau Proteins in N2a Cells. *Int. J. Nanomed.* **2020**, *Volume 15*, 6779−6789.
(12) Jiang, Y.; Gao, H.; Turdu, G. Traditional Chinese medicinal herbs as potential AChE inhibitors for anti-Alzheimer's disease: A review. *Bioorg. Chem.* **2017**, *75*, 50−61.
(13) Fathi, E.; Katouli, F. H.; Riazi, G. H.; Shasaltaneh, M. D.; Parandavar, E.; Bayati, S.; Afrasiabi, A.; Nazari, R. The Effects of Alpha Boswellic Acid on Reelin Expression and Tau Phosphorylation in Human Astrocytes. *NeuroMol. Med.* **2017**, *19*, 136−146.
(14) Gomaa, A. A.; Makboul, R. M.; El-Mokhtar, M. A.; Abdel-Rahman, E. A.; Ahmed, I. A.; Nicola, M. A. Terpenoid-rich Elettaria cardamomum extract prevents Alzheimer-like alterations induced in diabetic rats via inhibition of GSK3β activity, oxidative stress and pro-inflammatory cytokines. *Cytokine.* **2019**, *113*, 405−416.
(15) Xu, Y.; Wei, H.; Gao, J. Natural Terpenoids as Neuro-inflammatory Inhibitors in LPS-stimulated BV-2 Microglia. *Mini-Rev. Med. Chem.* **2021**, *21*, 520−534.
(16) Haghaei, H.; Soltani, S.; Aref Hosseini, S.; Rashidi, M. R.; Karima, S. Boswellic Acids as Promising Leads in Drug Development against Alzheimera's Disease. *Pharm. Sci.* **2021**, *27*, 14−31.
(17) Jana, S.; Laha, B.; Maiti, S. Boswellia gum resin/chitosan polymer composites: Controlled delivery vehicles for aceclofenac. *Int. J. Biol. Macromol.* **2015**, *77*, 303−306.
(18) Mishra, S.; Bishnoi, R. S.; Maurya, R.; Jain, D. Boswellia Serrata ROXB.−a Bioactive Herb with Various Pharmacological Activities. *Asian J. Pharm. Clin. Res.* **2020**, 33−39.
(19) Yassin, N.; El-Shenawy, S.; Mahdy, K. A.; Gouda, N.; Marrie, A.; Farrag, A.; Ibrahim, B.; et al. Effect of Boswellia serrata on Alzheimeras disease induced in rats. *J. Arab Soc. Med. Res.* **2013**, *8*, 1−11.
(20) Mohamed, T. M.; Youssef, M. A. M.; Bakry, A. A.; El-Keiy, M. M. Alzheimer's disease improved through the activity of mitochondrial chain complexes and their gene expression in rats by boswellic acid. *Metab. Brain Dis.* **2021**, *36*, 255−264.
(21) Karima, O.; Riazi, G.; Khodadadi, S.; Yousefi, R.; Mahnam, K.; Mokhtari, F.; Cheraghi, T.; Hoveizi, E.; Moosavi-Movahedi, A. A. An in vitro study of the role of β-boswellic acid in the microtubule assembly dynamics. *FEBS Lett.* **2012**, *586*, 4132−4138.
(22) Karima, O.; Riazi, G.; Yousefi, R.; Movahedi, A. A. M. The enhancement effect of beta-boswellic acid on hippocampal neurites outgrowth and branching (an in vitro study). *Neurol. Sci.* **2010**, *31*, 315−320.
(23) Gaur, P. K.; Puri, D.; Singh, A. P.; Kumar, N.; Rastogi, S. Optimization and Pharmacokinetic Study of Boswellic Acid−Loaded Chitosan-Guggul Gum Nanoparticles Using Box-Behnken Experimental Design. *Journal of Pharmaceutical Innovation* **2022**, *17*, 485−500.
(24) Silva, S.; Almeida, A. J.; Vale, N. Acetylcholinesterase inhibitors and nanoparticles on Alzheimer's disease: a review. *J. Nanopart. Res.* **2021**, *23*, 9.
(25) Ouyang, Q.; Meng, Y.; Zhou, W.; Tong, J.; Cheng, Z.; Zhu, Q. New advances in brain-targeting nano-drug delivery systems for Alzheimer's disease. *J. Drug Targeting* **2022**, *30*, 61−81.
(26) Cano, A.; Turowski, P.; Ettcheto, M.; Duskey, J. T.; Tosi, G.; Sánchez-López, E.; García, M. L.; Camins, A.; Souto, E. B.; Ruiz, A. Nanomedicine-based technologies and novel biomarkers for the diagnosis and treatment of Alzheimer's disease: from current to future challenges. *J. Nanobiotechnol* **2021**, *19*, 122.
(27) Moore, K. A.; Pate, K. M.; Soto-Ortega, D. D.; Lohse, S.; van der Munnik, N.; Lim, M.; Jackson, K. S.; Lyles, V. D.; Jones, L.; Glassgow, N.; et al. Influence of gold nanoparticle surface chemistry and diameter upon Alzheimer's disease amyloid-β protein aggregation. *J. Biol. Eng.* **2017**, *11*, DOI: 10.1186/s13036-017-0047-6
(28) Yang, L.; Yin, T.; Liu, Y.; Sun, J.; Zhou, Y.; Liu, J. Gold nanoparticle-capped mesoporous silica-based H2O2-responsive controlled release system for Alzheimer's disease treatment. *Acta Biomater.* **2016**, *46*, 177−190.
(29) Govindarajan, A.; Gnanasambandam, V. Toward Intracellular Bioconjugation Using Transition-Metal-Free Techniques. *Bioconjugate Chem.* **2021**, *32*, 1431−1454.
(30) Botteon, C. E. A.; Silva, L. B.; Ccana-Ccapatinta, G. V.; Silva, T. S.; Ambrosio, S. R.; Veneziani, R. C. S.; Bastos, J. K.; Marcato, P. D. Biosynthesis and characterization of gold nanoparticles using Brazilian red propolis and evaluation of its antimicrobial and anticancer activities. *Sci. Rep.* **2021**, *11*, DOI: 10.1038/s41598-021-81281-w
(31) Nah, H.; Lee, D.; Lee, J. S.; Lee, S. J.; Heo, D. N.; Lee, Y.-H.; Bang, J. B.; Hwang, Y.-S.; Moon, H.-J.; Kwon, I. K. Strategy to inhibit effective differentiation of RANKL-induced osteoclasts using vitamin D-conjugated gold nanoparticles. *Appl. Surf. Sci.* **2020**, *527*, 146765.
(32) Jazayeri, M. H.; Amani, H.; Pourfatollah, A. A.; Pazoki-Toroudi, H.; Sedighimoghaddam, B. Various methods of gold nanoparticles (GNPs) conjugation to antibodies. *Sens. BioSensing Res.* **2016**, *9*, 17−22.
(33) Busch, R. T.; Karim, F.; Weis, J.; Sun, Y.; Zhao, C.; Vasquez, E. S. Optimization and Structural Stability of Gold Nanoparticle−Antibody Bioconjugates. *ACS Omega* **2019**, *4*, 15269−15279.

(34) Retout, M.; Blond, P.; Jabin, I.; Bruylants, G. Ultrastable PEGylated Calixarene-Coated Gold Nanoparticles with a Tunable Bioconjugation Density for Biosensing Applications. *Bioconjugate Chem.* **2021**, *32*, 290−300.
(35) Sonawane, S. K.; Ahmad, A.; Chinnathambi, S. Protein-Capped Metal Nanoparticles Inhibit Tau Aggregation in Alzheimer's Disease. *ACS Omega* **2019**, *4*, 12833−12840.
(36) Falahati, M.; Attar, F.; Sharifi, M.; Haertlé, T.; Berret, J.-F.; Khan, R. H.; Saboury, A. A. A health concern regarding the protein corona, aggregation and disaggregation. *Biochimica et Biophysica Acta (BBA) - General Subjects* **2019**, *1863*, 971−991.
(37) Arghavani, P.; Badiei, A.; Ghadami, S. A.; Habibi-Rezaei, M.; Moosavi-Movahedi, F.; Delphi, L.; Moosavi-Movahedi, A. A. Inhibiting mTTR Aggregation/Fibrillation by a Chaperone-like Hydrophobic Amino Acid-Conjugated SPION. *J. Phys. Chem. B* **2022**, *126*, 1640−1654.
(38) Hakimian, F.; Ghourchian, H.; Hashemi, A. s.; Arastoo, M. R.; Behnam Rad, M. Ultrasensitive optical biosensor for detection of miRNA-155 using positively charged Au nanoparticles. *Sci. Rep.* **2018**, *8*, DOI: 10.1038/s41598-018-20229-z
(39) Jara, N.; Milán, N. S.; Rahman, A.; Mouheb, L.; Boffito, D. C.; Jeffryes, C.; Dahoumane, S. A. Photochemical Synthesis of Gold and Silver Nanoparticles—A Review. *Molecules* **2021**, *26*, 4585.
(40) Dekhili, R.; Cherni, K.; Liu, H.; Li, X.; Djaker, N.; Spadavecchia, J. Aptamer−Gold(III) Complex Nanoparticles: A New Way to Detect Cu, Zn SOD Glycoprotein. *ACS Omega* **2020**, *5*, 13851−13859.
(41) Schreiber, C. L.; Smith, B. D. Molecular conjugation using non-covalent click chemistry. *Nature Reviews Chemistry* **2019**, *3*, 393−400.
(42) Shelembe, B.; Mahlangeni, N. T.; Moodley, R. Biosynthesis of gold nanoparticles using monosaccharides of Artemisia afra and their antioxidant and anticancer properties. *Advances in Natural Sciences: Nanoscience and Nanotechnology* **2019**, *10*, 045002.
(43) Azmi, S. N. H.; Al-Jassasi, B. M. H.; Al-Sawafi, H. M. S.; Al-Shukaili, S. H. G.; Rahman, N.; Nasir, M. Optimization for synthesis of silver nanoparticles through response surface methodology using leaf extract of Boswellia sacra and its application in antimicrobial activity. *Environ. Monit. Assess* **2021**, *193*, 497.
(44) Thambiraj, S.; Vijayalakshmi, R.; Ravi Shankaran, D. An effective strategy for development of docetaxel encapsulated gold nanoformulations for treatment of prostate cancer. *Sci. Rep.* **2021**, *11*, 2808.
(45) Madhavan, A. A.; Juneja, S.; Moulick, R. G.; Bhattacharya, J. Growth Kinetics of Gold Nanoparticle Formation from Glycated Hemoglobin. *ACS Omega* **2020**, *5*, 3820−3827.
(46) Wu, B.-H.; Chung, J.-Y.; Hung, L.-Y.; Cheng, M.-C.; Peng, S.-M.; Chen, I.-C. Facet-Dependent Reduction Reaction of Diruthenium Metal−String Complexes by Face-to-Face Linked Gold Nanocrystals. *ACS Omega* **2019**, *4*, 5327−5334.
(47) Lee, H.; Hong, Y.; Lee, D.; Hwang, S.; Lee, G.; Yang, J.; Yoon, D. S. Surface potential microscopy of surfactant-controlled single gold nanoparticle. *Nanotechnology* **2020**, *31*, 215706.
(48) Aghaz, F.; Vaisi-Raygani, A.; Khazaei, M.; Arkan, E.; sajadimajd, S.; mozafari, H.; Rahimi, Z.; Pourmotabbed, T. Co-encapsulation of Tertinoin and Resveratrol by solid lipid nanocarrier (SLN) improves mice in vitro matured oocyte/ morula-compact stage embryo development. *Theriogenology* **2021**, *171*, 1.
(49) Consoli, G. M. L.; Tosto, R.; Baglieri, A.; Petralia, S.; Campagna, T.; Di Natale, G.; Zimbone, S.; Giuffrida, M. L.; Pappalardo, G. Novel Peptide-Calix [4] arene Conjugate Inhibits Aβ Aggregation and Rescues Neurons from Aβs Oligomers Cytotoxicity In Vitro. *ACS Chem. Neurosci.* **2021**, *12*, 1449−1462.
(50) Shoffner, S. K.; Schnell, S. Estimation of the lag time in a subsequent monomer addition model for fibril elongation. *Phys. Chem. Chem. Phys.* **2016**, *18*, 21259−21268.
(51) Tiwari, N. S.; van der Schoot, P. Stochastic lag time in nucleated linear self-assembly. *J. Chem. Phys.* **2016**, *144*, 235101.
(52) Rafiee, S.; Asadollahi, K.; Riazi, G.; Ahmadian, S.; Saboury, A. A. Vitamin B12 Inhibits Tau Fibrillization via Binding to Cysteine Residues of Tau. *ACS Chem. Neurosci.* **2017**, *8*, 2676−2682.
(53) Desale, S. E.; Dubey, T.; Chinnathambi, S. α-Linolenic acid inhibits Tau aggregation and modulates Tau conformation. *Int. J. Biol. Macromol.* **2021**, *166*, 687−693.
(54) Wallin, C.; Hiruma, Y.; Wärmländer, S. K. T. S.; Huvent, I.; Jarvet, J.; Abrahams, J. P.; Gräslund, A.; Lippens, G.; Luo, J. The neuronal tau protein blocks in vitro fibrillation of the amyloid-β (Aβ) peptide at the oligomeric stage. *J. Am. Chem. Soc.* **2018**, *140*, 8138−8146.
(55) Schartner, J.; Nabers, A.; Budde, B.; Lange, J.; Hoeck, N.; Wiltfang, J.; Kötting, C.; Gerwert, K. An ATR−FTIR Sensor Unraveling the Drug Intervention of Methylene Blue, Congo Red, and Berberine on Human Tau and Aβ. *ACS Med. Chem. Lett.* **2017**, *8*, 710−714.
(56) Ukmar-Godec, T.; Fang, P.; Ibanez de Opakua, A.; Henneberg, F.; Godec, A.; Pan, K.-T.; Cima-Omori, M.-S.; Chari, A.; Mandelkow, E.; Urlaub, H.; Zweckstetter, M. Proteasomal degradation of the intrinsically disordered protein tau at single-residue resolution. *Sci. Adv.* **2020**, *6*, DOI: 10.1126/sciadv.aba3916
(57) Saha, B.; Chowdhury, S.; Sanyal, D.; Chattopadhyay, K.; Suresh Kumar, G. Comparative Study of Toluidine Blue O and Methylene Blue Binding to Lysozyme and Their Inhibitory Effects on Protein Aggregation. *ACS Omega* **2018**, *3*, 2588−2601.
(58) Mahmoudi, M.; Kalhor, H. R.; Laurent, S.; Lynch, I. Protein fibrillation and nanoparticle interactions: opportunities and challenges. *Nanoscale* **2013**, *5*, 2570.
(59) Zarei, M.; Aalaie, J. Profiling of nanoparticle−protein interactions by electrophoresis techniques. *Anal. Bioanal. Chem.* **2019**, *411*, 79−96.
(60) Ramesh, N. K.; Sudhakar, S.; Mani, E. Modeling of the Inhibitory Effect of Nanoparticles on Amyloid β Fibrillation. *Langmuir* **2018**, *34*, 4004−4012.
(61) Fichou, Y.; Lin, Y.; Rauch, J. N.; Vigers, M.; Zeng, Z.; Srivastava, M.; Keller, T. J.; Freed, J. H.; Kosik, K. S.; Han, S. Cofactors are essential constituents of stable and seeding-active tau fibrils. *Proc. Natl. Acad. Sci. U. S. A* **2018**, *115*, 13234−13239.
(62) Jangholi, A.; Ashrafi-Kooshk, M. R.; Arab, S. S.; Riazi, G.; Mokhtari, F.; Poorebrahim, M.; Mahdiuni, H.; Kurganov, B. I.; Moosavi-Movahedi, A. A.; Khodarahmi, R. Appraisal of role of the polyanionic inducer length on amyloid formation by 412-residue 1N4R Tau protein: A comparative study. *Arch. Biochem. Biophys.* **2016**, *609*, 1−19.
(63) Ramshini, H.; Moghaddasi, A.-S.; Mollania, N.; Khodarahmi, R. Diverse antithetical effects of the bio-compatible Ag-NPs on the hen egg lysozyme amyloid aggregation: from an efficient inhibitor to obscure inducer. *J. Iran. Chem. Soc.* **2019**, *16*, 33−44.
(64) Mahmoudi, M.; Quinlan-Pluck, F.; Monopoli, M. P.; Sheibani, S.; Vali, H.; Dawson, K. A.; Lynch, I. Influence of the Physiochemical Properties of Superparamagnetic Iron Oxide Nanoparticles on Amyloid β Protein Fibrillation in Solution. *ACS Chem. Neurosci* **2013**, *4*, 475−485.
(65) Lotfabadi, A.; Hajipour, M. J.; Derakhshankhah, H.; Peirovi, A.; Saffar, S.; Shams, E.; Fatemi, E.; Barzegari, E.; Sarvari, S.; Moakedi, F.; Ferdousi, M.; Atyabi, F.; Saboury, A. A.; Dinarvand, R. Biomolecular Corona Dictates Aβ Fibrillation Process. *ACS Chem. Neurosci.* **2018**, *9*, 1725−1734.
(66) Pasieka, A.; Panek, D.; Szałaj, N.; Espargaró, A.; Więckowska, A.; Malawska, B.; Sabaté, R.; Bajda, M. Dual Inhibitors of Amyloid-β and Tau Aggregation with Amyloid-β Disaggregating Properties: Extended In Cellulo, In Silico, and Kinetic Studies of Multifunctional Anti-Alzheimers Agents. *ACS Chem. Neurosci.* **2021**, *12*, 2057−2068.
(67) Sonawane, S. K.; Chidambaram, H.; Boral, D.; Gorantla, N. V.; Balmik, A. A.; Dangi, A.; Ramasamy, S.; Marelli, U. K.; Chinnathambi, S. EGCG impedes human Tau aggregation and interacts with Tau. *Sci. Rep* **2020**, *10*, 12579.
(68) Ojaghi, S.; Mohammadi, S.; Amani, M.; Ghobadi, S.; Bijari, N.; Esmaeili, S.; Khodarahmi, R. Sunset yellow degradation product, as an

efficient water-soluble inducer, accelerates 1N4R Tau amyloid oligomerization: In vitro preliminary evidence against the food colorant safety in terms of "Triggered Amyloid Aggregation. *Bioorg. Chem.* **2020**, *103*, 104123.
(69) Bijari, N.; Balalaie, S.; Akbari, V.; Golmohammadi, F.; Moradi, S.; Adibi, H.; Khodarahmi, R. Effective suppression of the modified PHF6 peptide/1N4R Tau amyloid aggregation by intact curcumin, not its degradation products: Another evidence for the pigment as preventive/therapeutic "functional food. *Int. J. Biol. Macromol.* **2018**, *120*, 1009−1022.
(70) John, T.; Gladytz, A.; Kubeil, C.; Martin, L. L.; Risselada, H. J.; Abel, B. Impact of nanoparticles on amyloid peptide and protein aggregation: a review with a focus on gold nanoparticles. *Nanoscale* **2018**, *10*, 20894−20913.
(71) Tapia-Arellano, A.; Gallardo-Toledo, E.; Celis, F.; Rivera, R.; Moglia, I.; Campos, M.; Carulla, N.; Baez, M.; Kogan, M. J. The curvature of gold nanoparticles influences the exposure of amyloid-β and modulates its aggregation process. *Mater. Sci. Eng. C Mater. Biol. Appl.* **2021**, *128*, 112269.
(72) Caballero, A. B.; Gamez, P. Nanochaperone-Based Strategies to Control Protein Aggregation Linked to Conformational Diseases. *Angew. Chem.* **2021**, *133*, 41−52.
(73) Jangholi, A.; Ashrafi-Kooshk, M. R.; Arab, S. S.; Karima, S.; Poorebrahim, M.; Ghadami, S. A.; Moosavi-Movahedi, A. A.; Khodarahmi, R. Can any "non-specific charge modification within microtubule binding domains of Tau" be a prerequisite of the protein amyloid aggregation? An in vitro study on the 1N4R isoform. *Int. J. Biol. Macromol.* **2018**, *109*, 188−204.
(74) Stopschinski, B. E.; Thomas, T. L.; Nadji, S.; Darvish, E.; Fan, L.; Holmes, B. B.; Modi, A. R.; Finnell, J. G.; Kashmer, O. M.; Estill-Terpack, S.; Mirbaha, H.; Luu, H. S.; Diamond, M. I. A synthetic heparinoid blocks Tau aggregate cell uptake and amplification. *J. Biol. Chem.* **2020**, *295*, 2974−2983.

https://doi.org/10.1021/acsomega.2c03616
ACS Omega 2022, 7, 30347−30358